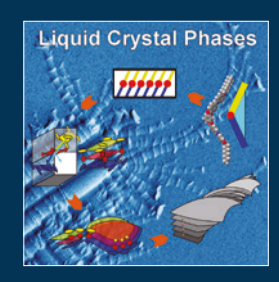
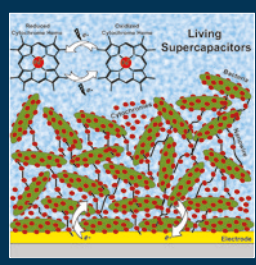
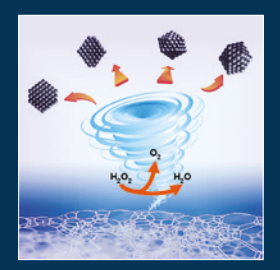
### A EUROPEAN JOURNAL

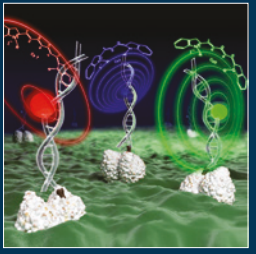
# CHEMPHYSCHEM

## OF CHEMICAL PHYSICS AND PHYSICAL CHEMISTRY

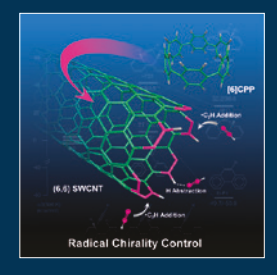


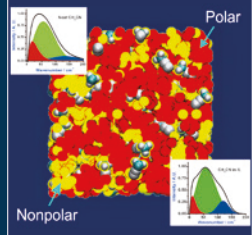






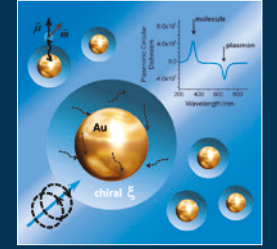


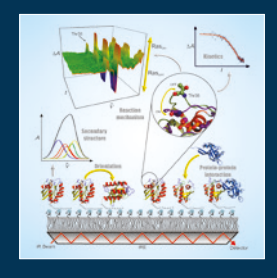


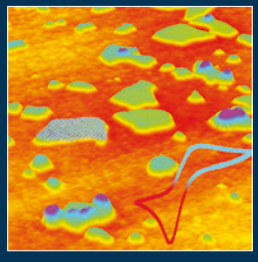


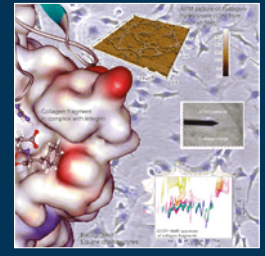




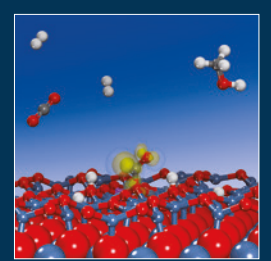


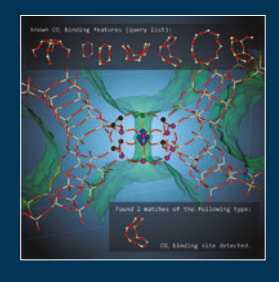
















# Reprint

© Wiley-VCH Verlag GmbH & Co. KGaA, Weinheim





DOI: 10.1002/cphc.201800855





# Metal-ion Binding to Host Defense Peptide Piscidin 3 Observed in Phospholipid Bilayers by Magic Angle **Spinning Solid-state NMR**

Ratan Kumar Rai, [c] Anna De Angelis, [c] Alexander Greenwood, [b] Stanley J. Opella, [c] and Myriam L. Cotten\*[a]

Cationic antimicrobial peptides (AMPs) are essential components of the innate immune system. They have attracted interest as novel compounds with the potential to treat infections associated with multi-drug resistant bacteria. In this study, we investigate piscidin 3 (P3), an AMP that was first discovered in the mast cells of hybrid striped bass. Prior studies showed that P3 is less active than its homolog piscidin 1 (P1) against planktonic bacteria. However, P3 has the advantage of being less toxic to mammalian cells and more active on biofilms and persister cells. Both P1 and P3 cross bacterial membranes and co-localize with intracellular DNA but P3 is more condensing to DNA while P1 is more membrane active. Recently, we showed that both peptides coordinate Cu<sup>2+</sup> through an aminoterminal copper and nickel (ATCUN) motif. We also demonstrated that the bactericidal effects of P3 are linked to its ability to form radicals that nick DNA in the presence of Cu<sup>2+</sup>. Since metal binding and membrane crossing by P3 is biologically important, we apply in this study solid-state NMR spectroscopy to uniformly <sup>13</sup>C-<sup>15</sup>N-labeled peptide samples to structurally characterize the ATCUN motif of P3 bound to bilayers and coordinated to Ni<sup>2+</sup> and Cu<sup>2+</sup>. These experiments are supplemented with density functional theory calculations. Taken together, these studies refine the arrangement of not only the backbone but also side chain atoms of an AMP simultaneously bound to metal ions and phospholipid bilayers.

#### 1. Introduction

The study of amphipathic  $\alpha$ -helical peptides as components of the vertebrate immune system was initiated by Zasloff's discovery of the antibiotic activity of 23-residue magainins in frog skin.[1] This was preceded by the identification of 37-residue cecropin peptides in insects, which have similar structural features and antibiotic activities. [2] With obvious relevance to the treatment of infectious diseases, many natural and synthetic variants of these antimicrobial peptides (AMPs) have been characterized. [3,4] Much of the interest in these peptides results from their potential to address the increase in antibiotic resistance by human pathogens.<sup>[5]</sup> In contrast to conventional antibiotics that act through specific interactions with welldefined, high-affinity targets, AMPs rely on low-affinity interactions with bacterial cell membranes.<sup>[6-10]</sup> As the archetypical AMP, magainin has been subjected to extensive NMR studies in a variety of membrane mimetic environments including nearnative phospholipid bilayers.[11-19] Complementary results from other biophysical approaches have led to models for its mechanism of action, most of which focus on its ability to form ion channels in membranes. In recent years, it has been recognized that following their initial interactions with bacterial cell membranes, some AMPs may translocate across the membrane and affect intracellular targets, such as DNA.[10,20] The membrane activity of such AMPs arises from their cell penetrating properties rather than their ability to permeabilize and lyse bacterial membranes. In addition to their direct attack of bacteria, some AMPs have immunomodulatory effects that involve activating host cells to boost the immune response. [21-24]

Piscidins were the first antimicrobial cationic peptides isolated from the mast cells of hybrid striped bass. [25] These 22residue peptides have broad-spectrum activity against many pathogens, including multidrug-resistant bacteria, fungi, and viruses. [26] Piscidin 1 (P1, FFHHIFRGIVHVGKTIHRLVTG) and Piscidin 3 (P3, FIHHIFRGIVHAGRSIGRFLTG) have similar sequences but are differentially expressed; although they are highly potent, their biological activities differ for unknown reasons.[27] While P1 has stronger antimicrobial activity than P3 against some planktonic bacteria, P3 has higher specificity. [26] Both peptides translocate across the membranes of cells, leading to co-localization with intracellular DNA.[27]

We previously used oriented sample solid-state NMR to solve the structures and orientations of P1 and P3 bound to bacterial cell mimics.<sup>[28]</sup> These structures, which were deposited in the protein data bank (PDB), indicated that membrane-bound P1 and P3 are structurally similar. Both peptides form  $\alpha$ -helical

E-mail: mcotten@wm.edu

[b] Dr. A. Greenwood Department of Applied Science and Department of Physics, The College of William and Mary Williamsburg, VA 23185 (USA)

[c] Dr. R. K. Rai, Dr. A. De Angelis, Prof. S. J. Opella Department of Chemistry and Biochemistry University of California San Dieao La Jolla, California 92093-0307 (USA)



An invited contribution to a Special Issue on BioNMR Spectroscopy

<sup>[</sup>a] Prof. M. L. Cotten Department of Applied Science, The College of William and Mary Williamsburg, VA 23185 (USA) Fax: (757)-221-2050





structures that are kinked at a central glycine (G13) and oriented parallel to the bilayer surface. Notably, the kink at Gly13 allows both amphipathic peptides to maximize their hydrophobic moment, as needed to optimize their hydrophobic interactions with the nonpolar core of the membrane. While the first three residues were noted to have  $\alpha\text{-helical}$  character, this part of the  $\alpha\text{-helix}$  was frayed due to weaker hydrogen bonding.

Recently, we demonstrated that the N-termini of both peptides coordinate  $Cu^{2+}$  through their amino-terminal copper and nickel (ATCUN) motif of consensus sequence XXH, where X can be any amino acid. This motif, which is FFH- for P1 and FIH- for P3, binds to  $Cu^{2+}$  and  $Ni^{2+}$  ions with high affinity. The N-terminal amino group, the two subsequent backbone amide nitrogens, and the  $\delta$ -nitrogen of His3 form the metal-binding site, which has a square planar coordination geometry. Upon metal binding, reactive oxygen species (ROS) are formed through Fenton-like chemical reactions. By applying solution NMR to  $^{15}$ N3-H3 labelled P3, we were able to demonstrate that the side chain of H3 is involved in metal coordination.

Our studies have shown that the antimicrobial effects of P1 are instantaneous; by contrast, it requires about one hour for those of P3 to become noticeable.<sup>[29]</sup> These findings correlate with P1 being more membrane permeabilizing than P3 and P3 being more effective at condensing DNA and faster at cleaving isolated DNA.<sup>[26]</sup> Furthermore, in living cells P3 has stronger copper-scavenging nuclease activities than P1.<sup>[26]</sup> Further, P3 differs from P1 by having arginine instead of lysine at position 14. Molecular dynamics (MD) simulations show that this arginine mediates stronger interactions with DNA than the lysine in P1.<sup>[26]</sup> The picture emerging from these results is that the bactericidal activities of P3 are linked to its ability to translocate across bacterial cell membranes in order to access intracellular DNA and affect it physically through aggregation and chemically through bond cleavage.

Here, we extend the characterization of the metal binding site of P3 to additional residues using solid-state NMR and gain new insights into the structure of P3 bound to not only a metal ion but also bilayers. We apply solid-state NMR spectroscopy to samples of uniformly <sup>13</sup>C/<sup>15</sup>N-labeled P3. The experimental results describe the structural effects of binding metal ions to P3 associated with phospholipid bilayers. The chosen bilayers feature a mixture of lipids similar to those found in the bacterial cell membranes that P3 interacts with in the initial stages of its mechanism of action. We also present density functional theory (DFT) calculations to gain new insights into the structural changes taking place at the amino terminus of the peptide upon metal coordination. Significantly, Ni<sup>2+</sup> and Cu<sup>2+</sup> are known to colocalize with AMPs on the surface of bacterial cells as part of the immune response. [27] Therefore, it may be possible to deduce from these NMR and DFT studies the roles of metalpeptide complexes in the mechanism of antibiotic activities by the peptide.

#### 2. Results and Discussion

It is well established that chemical shift frequencies of individual resonances are affected by the local electronic environment, and can thus provide local structural and dynamic information.[31-34] In particular, the binding of metal ions to specific residues affects the NMR resonances of proximate residues. Since Cu2+ has unpaired electrons, the associated paramagnetic effects strongly influence both the chemical shifts and the relaxation rates of resonances from nearby sites. The shortening of relaxation rates by paramagnetic effects leads to the loss of NMR signals from sites located less than about 10 Å from the metal. Here, we take advantage of the paramagnetic effects of Cu<sup>2+</sup> to characterize the folding of the amino terminal residues of P3 upon metal binding. We also performed experiments on peptides bound to diamagnetic Ni<sup>2+</sup>, which has previously been shown to bind the ATCUN motif in a manner structurally similar to that of Cu<sup>2+</sup>. By comparison, this enabled us to measure the paramagnetic effects of bound Cu<sup>2+</sup>. [35]

The photographs of the peptide-containing proteoliposome pellets in Figure 1 vividly display the colors associated with the binding of different metals to P3 in lipid bilayers constituted of 3:1 1,2-dimyristoyl-sn-glycero-3-phosphocholine (DMPC)/1,2-dimyristovl-sn-alycero-3-phosphoalycerol (DMPG). The apo-P3 sample is white; in contrast, the metal-containing P3 samples are yellow and pink, reflecting absorbance of light at 420 and 525 nm by the nickel- and copper-coordinated peptide, respectively.[36,37] The solid-state NMR spectra of all three P3 samples are well-resolved. This is demonstrated by the twodimensional <sup>13</sup>C/<sup>13</sup>C correlation spectrum of Ni<sup>2+</sup>-bound P3 shown in Figure 2A. The <sup>13</sup>C resonances have linewidths at half height of ~0.6 ppm. With a 10 ms mixing time, primarily crosspeaks from one-bond correlations are observed, although some signals from weak two-bond correlations are present. With a 50 ms mixing time, the signals from two- and three-bond correlations are more clearly observable in the spectra. A twodimensional N-CA spectrum is shown in Figure 3A. A detailed analysis of <sup>13</sup>C/<sup>13</sup>C correlation spectra obtained with 10 ms, 20 ms, 50 ms, 100 ms mixing times for proton driven spin diffusion (PDSP) as well as NCA and NCO spectra provide the resonance assignments marked in the spectra in Figures 2A and

Paramagnetic  $Cu^{2+}$  strongly enhances the relaxation of proximal nuclei. This identifies the location of the metal binding site. As shown in Figure 3 and Figure 4 A, signals from residues

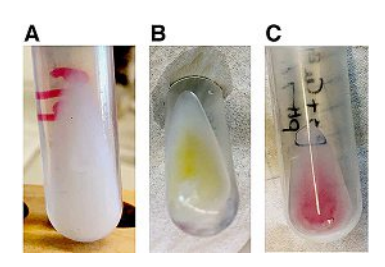


Figure 1. DMPC/DMPG proteoliposome samples for a 20:1 molar ratio of lipid at pH 7.4: A) apo-P3, B)  $\rm Ni^{2^+}$ -, and C)  $\rm Cu^{2^+}$ -bound P3.

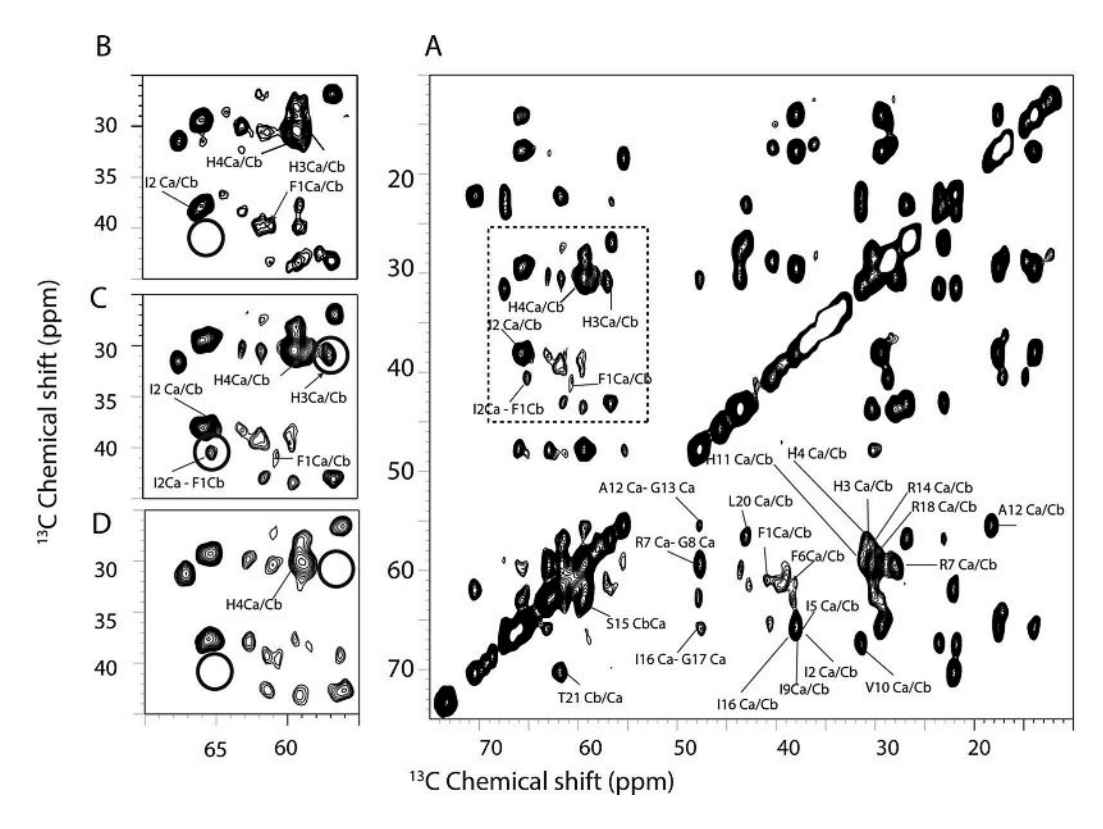


Figure 2. Two-dimensional  $^{13}$ C— $^{13}$ C MAS spectra of uniformly  $^{13}$ C/ $^{15}$ N labeled P3 in DMPC proteoliposomes at 7 °C. All these spectra were acquired with 256 scans and a 50 ms mixing time. A) 2D homonuclear  $^{13}$ C/ $^{13}$ C spin-exchange correlation spectrum of P3 bound to Ni<sup>2+</sup>. Zoomed regions for spectra of apo, Ni<sup>2+</sup> and Cu<sup>2</sup>-bound P3 are represented in (B), (C), and (D). The experiments were performed at 750 MHz under 11.11 kHz MAS.

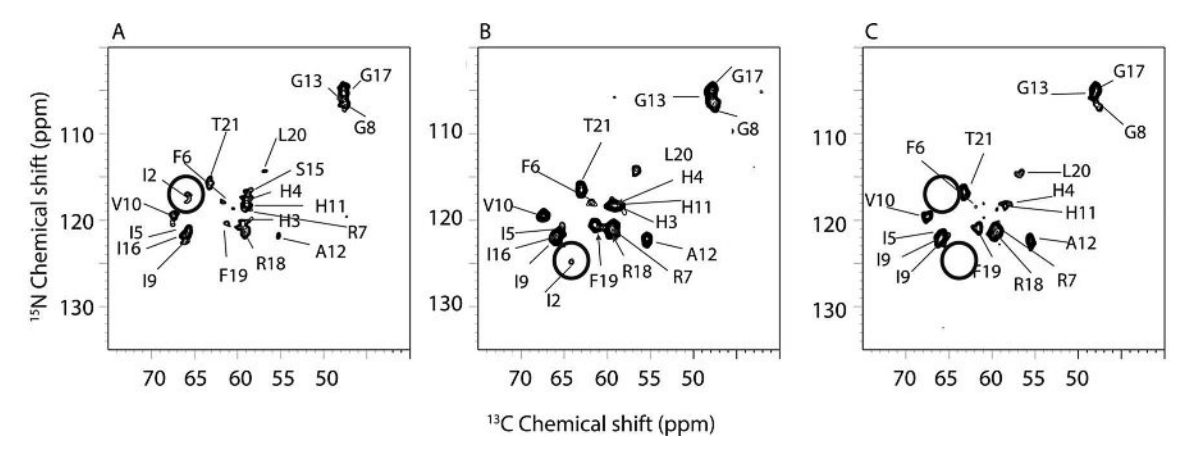
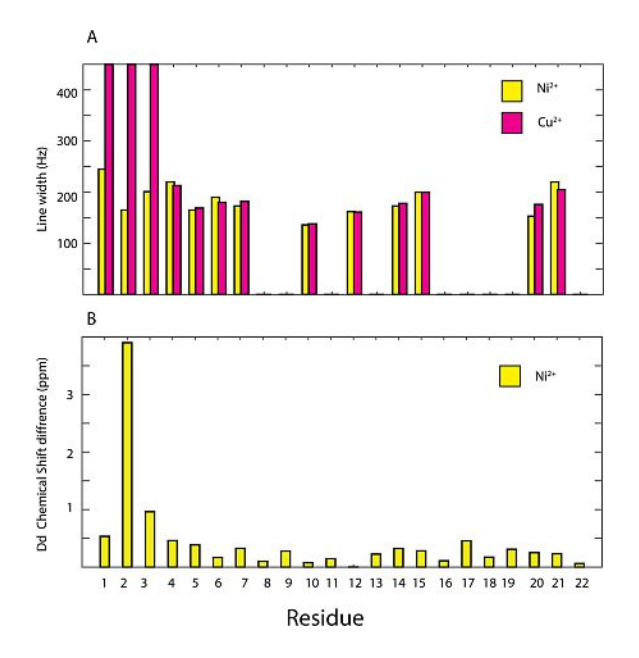


Figure 3. Two-dimensional heteronuclear <sup>13</sup>C/<sup>15</sup>N correlation spectrum of P3. A) apo-P3, B) Ni<sup>2+</sup>-bound P3, C) Cu<sup>2+</sup>-bound P3.

1, 2, and 3 are broadened beyond detection; as monitored by the signal intensities of other resonances, the metal ion has little or no effect on other residues in the peptide, including residue 4. In contrast to the dramatic effects of Cu<sup>2+</sup> at the amino terminus of P3, the binding of diamagnetic Ni<sup>2+</sup> to P3 does not abrogate the signals from residues 1, 2 and 3. However, some minor changes in line widths (and signal intensities) are detected for the first seven residues, F1, I2, H3, H4, I5, F6, and R7. Interestingly, metal binding affects the signals of several residues near the C-terminal end of P3. For

instance, the crosspeak for F19 becomes more intense upon metallation (Figure 3) while its line width is unaffected (Figure 4 B). In addition, the line widths increase for L19 and T21 (Figure 4). These effects suggest that metal binding is sensed at the C-terminal end of P3, possibly due to intermolecular interactions mediated by hydrophobic residues present at the two extremities of P3, such as F1, I2, I5, F6, F19 and L20.

Inspection of the expanded regions of the spectra in Figures 2 and 3 demonstrate differences in the signals from the first three residues of P3. The magnitudes of metal-induced

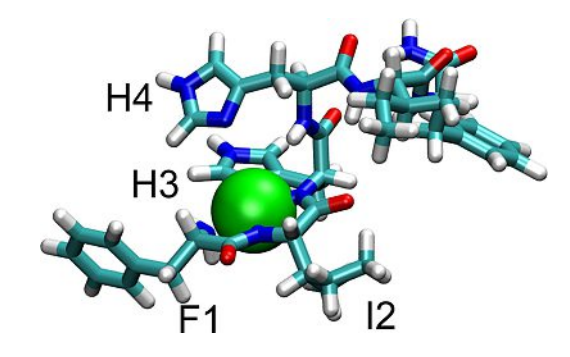


**Figure 4.** A) Comparison of line widths between Ni<sup>2+</sup>-bound (yellow) and Cu<sup>2+</sup>-bound P3 (pink). The line widths were measured from two-dimensional <sup>13</sup>C/<sup>13</sup>C spectra obtained with a 10 ms mixing time. B) Chemical shift perturbations (i.e. CSDs) for <sup>13</sup>C and <sup>15</sup>N resonances upon Ni<sup>2+</sup> binding to P3.

chemical shift-perturbations are quantified with the well-established equation for chemical shift deviations (CSDs):  $\Delta\delta=1/2\sqrt{(\Delta\delta C/2)^2+(\Delta\delta N/5)^2} \text{ where } \Delta\delta C \text{ and } \Delta\delta N \text{ are the changes in carbon and nitrogen chemical shifts, respectively.}^{[38,39]} \text{ As shown in Figure 4B, there are significant chemical shift changes in both $^{13}$C and <math display="inline">^{15}$N$ resonances upon Ni$^{2+} coordination at the amino end of P3.}$ 

The ATCUN motif is found in many peptides and proteins. [29] The metal-bound ATCUN complexes have been shown to cleave DNA and RNA and inactivate enzymes. [40,41] The stability of the complex is governed by the basicity of the N-terminal amino group because of the competition between <sup>1</sup>H and Cu<sup>2+</sup> coordination. The Cu-ATCUN complex stability is significantly enhanced by bulky and hydrophobic amino acid residues at positions 1 and 2. [42] Notably, P3 has an isoleucine at position 2, whose resonances are strongly affected by metal ion binding as shown in Figure 4B wherethe resonances from I2 are marked by a circle.

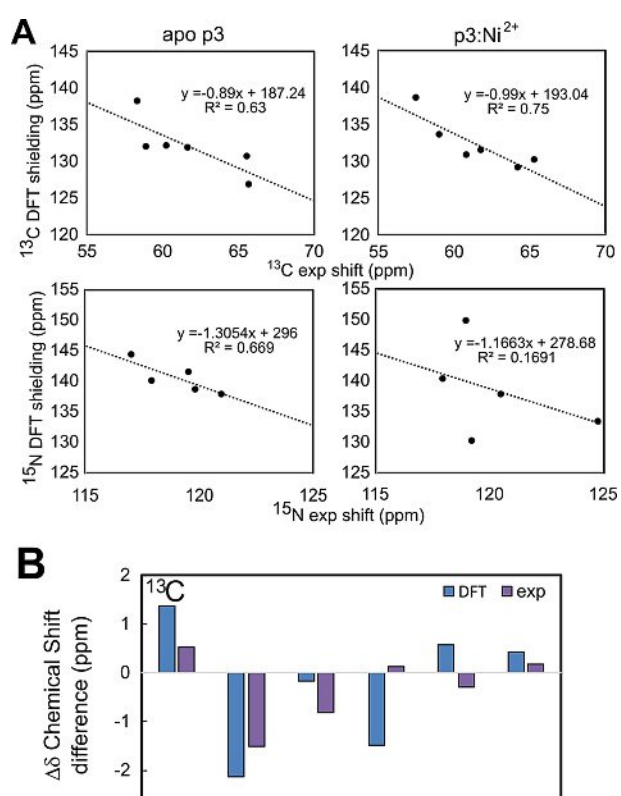
To further investigate the structure of the metallated ATCUN motif of P3, we performed DFT chemical shielding calculations on the first six residues of P3 in 3:1 DMPC:DMPG<sup>[28]</sup> and a model of P3-Ni<sup>2+</sup> based on the structure of the hexapeptide, FIHHIF. In this Ni<sup>2+</sup>-bound fragment of P3, the first three residues were modeled to coordinate Ni<sup>2+</sup> with their deprotonated backbone nitrogens (N-terminal amine and two amides), while the imidazole sidechain of H3 provided a fourth coordinating ligand, as needed to generate the square planar coordination geometry of the metallated ATCUN motif (Figure 5). Residues 4-onward were modeled as an  $\alpha$ -helix, similarly to the apo structure.<sup>[28]</sup> The results of DFT calculations are compared to the experimental shifts in Figure 6. In both the



**Figure 5.** Structure of the P3-Ni<sup>2+</sup> complex used in the DFT chemical shift calculations. The Ni<sup>2+</sup> ion (green sphere) is coordinated to the backbone nitrogens of F1, I2, and H3 as well as the imidazole sidechain of H3 in a square-planar geometry. The structure is consistent with bulky side chains (I2, H4) surrounding the metal ion.

metal-bound and apo tates, the calculated <sup>13</sup>C chemical shieldings are consistent with the observed shifts, showing a linear trend with a slope close to -1, as expected (Figure 6A, top). This leads to a reasonable correspondence when the experimental and DFT-derived <sup>13</sup>C CSDs are plotted for the metal-bound and apo-complexes (Figure 6B, top). Hence, the alpha carbon CSDs observed for the first three residues are consistent with the different dihedral angles adopted in the  $\alpha$ helix of the apo-state and the square-planar geometry of the Ni<sup>2+</sup>-bound state. Although <sup>15</sup>N shieldings, which are considerably more challenging to calculate accurately, [43] are not wellcorrelated to the experimental shifts (Figure 6A, bottom), the large shift difference for the amide nitrogen of I2 is observed (Figure 6B, bottom). This CSD is consistent with the nitrogen of 12 participating in the coordination of the Ni<sup>2+</sup> ion. Taken together, the DFT calculations provide a basis for interpreting the Ni<sup>2+</sup>-induced chemical shift changes and support a model in which the ATCUN motif of P3 binds Ni<sup>2+</sup> in a square-planar geometry, and the bulky 12 and H4 side chains surround the metal, while residues 4-22 do not experience signficant conformational changes, as shown in Figure 5.

In the apo-state, the amino terminus of P3 was previously shown to be slightly more inserted in the bilayer than the C-terminal end. [28] In the halo-state, metal coordination through the ATCUN-motif results in the net loss of one positive charge. Indeed, the amine at position 1 and the amide nitrogens at positions 2 and 3 drop one proton each, resulting in a neutral amine and two negatively charged amide nitrogens. [44,45] Since the metal brings two positive charges, the peptide experiences the loss of one positive charge. This decrease in charge toghether with the bulky I2 and H4 side chains surrounding the metal ion may facilitate the insertion of the peptide into the hydrophobic environment of the bilayer and enhance its ability to cross the membrane and reach the cytoplasm.



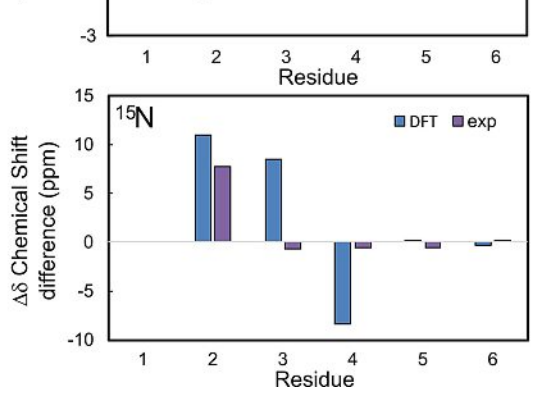


**Figure 6.** A) Comparison of experimental chemical shifts and calculated chemical shieldings for alpha carbons (top) and amide nitrogens (bottom). Plots for apo-P3 (left) and Ni<sup>2+</sup>-bound P3 (right) are shown. Symbols reflect data points and lines are linear regressions, with slopes/intercepts and R<sup>2</sup> values displayed above the plot. B) Comparison of experimental (purple) and DFT-derived (blue) CSDs between apo-P3 and Ni<sup>2+</sup>-bound P3. Data for alpha carbons (top) and amide nitrogens (bottom) are shown.

#### 3. Conclusions

The holo-state of P3, as studied here, is relevant to its natural environment and biological function. First, since AMPs such as P3 undergo post-translational modifications, including carboxyamidation, in several organelles (e.g. *trans*-Golgi apparatus) where copper ions are ubiquitous, [46] it is highly probable that piscidins exist in the metallated state before being secreted. In the pro-peptide form, piscidin features a sequence followed by the sequence GK. [47] This dipeptide is recognized by carboxypeptidase E and the  $\alpha$ -amidating monooxygenase (PAM) complex that remove GK sequences at the end of pro-peptides

and amidate their C-termini, as needed to generate mature peptides. [48,49] Since these post-translational modifications take place in organelles (e.g. *trans*-Golgi apparatus, secretory granules) where Cu<sup>2+</sup> is present and the PAM complex needs Cu<sup>2+</sup> for its function, [46,48] piscidins very likely bind Cu<sup>2+</sup> during these processing steps. Second, Cu<sup>2+</sup> ions play important roles as part of host defense and co-localize with AMPs such as P3 in cellular compartments, such as the phagosomes of immune cells. [50] Third, the bactericidal effects of P3 are enhanced by copper and synergistic effects exist between Cu<sup>2+</sup> and P3 on biofilms and persister cells. [26]

This study presents the first structural characterization of P3 simultaneously bound to a metal ion and bacterial cell mimics. Through a combination of solid-state NMR and DFT calculations, new insights are gained about the structure of the metal binding site, as shown in Figure 5. The first three residues form a square planar coordination geometry where the bulky side chains I2 and H4 surround the metal ion. This structural arrangement together with the net loss of one charge at the amino end of the peptide very likely play an important role in stabilizing the insertion of the N-terminus and metal ion in the hydrophobic core of the membrane it needs to cross in order to reach the cytoplasm. Our results also capture that the Cterminal end of P3 is sensitive to metal binding at the Nterminal end, possibly because intermolecular interactions taking place between multiple P3 molecules place the amino end of one peptide in proximity to the carboxylic end of another peptide.

Membrane binding is the first step in the mechanism of antimicrobial action by P3. It is followed by membrane crossing into the cytoplasm and DNA disruption. Given that P3 is expressed in vascularized tissues and exhibits low toxicity to host cells, its mechanism of action through membrane crossing followed by DNA cleavage catalyzed by metal binding may represent a novel form of specificity. The results described here provide insight into structural changes induced by metal coordination and serve to identify some of the specific structural features that help an AMP discriminate between host and invasive cells. The results may aid in the design of anti-infective agents that exhibit low toxicity to mammalian cells and high potency against bacterial pathogens, including those that are resistant to other classes of antibiotics.

#### **Experimental Section**

#### Peptide Synthesis, Purification, and Characterization

Chemicals were purchased from Sigma-Aldrich (Saint Louis, MO) unless otherwise indicated. \$^{15}C/^{15}N\$-labeled P3 (MW 2645 with labels) was synthesized from uniformly \$^{15}C/^{15}N\$-labeled amino acids using Fmoc-solid-phase peptide synthesis at the University of Texas Southwestern Medical Center. The peptide was purified by reverse phase HPLC as previously described. \$^{28}\$ Following HPLC, the peptide was washed with dilute HCl, lyophilized, and dialyzed to remove residual trifluoroacetic acid (TFA). The peptide was assessed as 98% pure by mass spectrometry.





#### **Proteoliposome Samples**

For all samples the molar peptide-to-lipid ratio (P/L) was 1:20 and the molar PC (Phosphatidylcholine) to PG (Phosphoglycerate) ratio was 3:1. The lipids were obtained from Avanti Polar Lipids (Alabaster, Alabama). The samples were prepared by co-dissolving DMPC and DMPG in a mixture of 2,2,2-trifluorethanol (TFE) and chloroform (50/50, v/v). Each sample contained approximately 4 mg of P3, after excluding an estimated 25% weight to account for the counter ions as measured by mass spectroscopy.

For apo-P3 samples ions (Figure 1A) the lipids were added to a round bottom glass tube containing the peptide dissolved in TFE. The solution was dried by passage of N<sub>2</sub> gas. After lyophilization, the film of peptide and lipids was rehydrated with 6 mL of 20 mM HEPES at pH 7.3, warmed to about 40 °C and gently mixed by vortexing and pipetting. The pH was adjusted to 7.4 with NaOH. The sample was swirled/vortexed gently to enable complete mixing of the peptide, lipids, and buffer. Next, the sample was ultracentrifuged in a Beckman Optima-90 K centrifuge at 90,000 rpm (644,000 g, Beckman NVT90 rotor) at 10 °C for 17 hours. Following centrifugation, the supernatant was removed and the pellet (Figure 1A) was recovered for the NMR experiments. Pellet hydration was found to be over 10-fold in weight, therefore the pellet size was reduced by lyophilizing for three hours and then re-hydrated with water to yield a 200 µL-sample. The final HEPES buffer concentration in the NMR sample was estimated to be at or below 80 mM, and the final water content was about 1.5 times the lipid

For proteoliposome samples containing metal ions (Figure 1B and 1C), the dry P3 peptide was first dissolved in ~2 mL of water, then mixed with an equimolar amount of either NiCl<sub>2</sub> or CuSO<sub>4</sub> in standardized aqueous solutions (Hampton Research, Aliso Viejo, CA for NiCl<sub>2</sub> and Ricca Chemicals, Pocomoke City, MD for CuSO<sub>4</sub>), resulting in clear colorless solutions at pH 5.5 (NiCl<sub>2</sub>) and 3.5 (CuSO<sub>4</sub>). The pH was adjusted to 7.4 using NaOH in both cases. As metal ions bind to P3 and displace protons, the solution pH decreases, with characteristically slow kinetics, [51] therefore this process takes several minutes. Above pH 7, metal-containing piscidin solutions displayed a typical yellow (nickel) or pink (copper) coloration, which provided an immediate visual test for metal binding. Indeed, ATCUN peptides bound to Ni<sup>2+</sup> and Cu<sup>2+</sup> absorb near 420 and 525 nm, respectively. [36,37,52] The distinctive colors were retained in the proteoliposome pellets (Figure 1). The solutions were then diluted to a volume of 6 mL before being added to the lipids, following the same sequence of steps as for the apo-P3 sample. The final pH was 7.4. The samples were then ultracentrifuged as described above, yielding the pellets shown in Figure 1B and 1C. These were lyophilized and rehydrated to prepare the samples used for MAS solid-state NMR spectroscopy.

#### Solid-state NMR Experiments

All of the solid-state NMR experiments were performed on a Bruker AVANCE-III HD 750 MHz spectrometer with a 4 mm H/C/N triple-resonance Bruker E-free MAS probe (Bruker https://www.bruker.com). The spinning rate was maintained at 11.11 kHz $\pm 2$  Hz and the temperature controller was set to  $7\pm 2\,^{\circ}\text{C}$ ; taking into account frictional heating and calibration with the  $^{1}\text{H}$  chemical shift of the water resonance the actual sample temperature is estimated to be  $10\pm 2\,^{\circ}\text{C}$ . The applied radiofrequency (rf) fields corresponded to  $\pi/2$  pulse lengths of 2.5  $\mu s$ , 3.2  $\mu s$  and 5.1  $\mu s$  for  $^{1}\text{H}$ ,  $^{13}\text{C}$  and  $^{15}\text{N}$ , respectively. The peptide-containing proteoliposome pellets were packed into 4 mm zirconia rotors containing teflon inserts and sealed with Vespel drive caps.

During direct <sup>13</sup>C detection, 100 kHz rf irradiation was used for <sup>1</sup>H decoupling with swept frequency two-pulse phase modulation (SW-TPPM). [53] Cross-polarization (CP)[54] from <sup>1</sup>H to <sup>15</sup>N was optimized using amplitude-modulated rf irradiation (100%-70%) applied on the <sup>1</sup>H channel; 50 kHz rf irradiation on the <sup>1</sup>H and ~27 kHz rf irradiation on the <sup>15</sup>N channels were applied during the 1 ms contact time. Two-dimensional PDSD pulse sequence with 10 ms, 50 ms, and 100 ms mixing times. [55-57] Double CP from 15N amide to <sup>13</sup>CA sites using spectrally induced filtering in combination with CP (SPECIFIC-CP). [58] Adiabatic tangential pulses were applied on the <sup>13</sup>C channel. For two-dimensional N–C correlation, rf irradiations of  $\sim 27 \text{ kHz}$  were applied on the  $^{15}\text{N}$  channel and ~16 kHz on the <sup>13</sup>C channel for band-selective polarization transfer and continuous wave <sup>1</sup>H irradiation (100 kHz rf field strength) was applied for decoupling during the 4.5 ms contact time for N-CA and N-CO transfers. The chemical shift frequencies were referenced externally to the adamantane methylene 13C resonance at 38.48 ppm and the ammonium sulfate <sup>15</sup>N resonance at 26.8 ppm.

#### **Density Functional Theory Calculations**

Two structures of the first 6 residues of P3 were used for DFT calculations: an apo structure based on the structure of P3 in 3:1 DMPC:DMPG<sup>[28]</sup> (PDB ID 2mcw), and a Ni<sup>2+</sup>-bound structure also derived from it. To generate the apo structure, the first six residues of 2mcw were extracted and the C-terminus was amidated in Avogadro. [59] The sidechain torsion angles of 15 were adjusted to better match the experimental <sup>13</sup>C shift of this residue. This structure was subjected to a geometry optimization in Gaussian 09, [60] keeping the phi and psi torsion angles for all residues fixed using the ModRedundant option. To generate the Ni<sup>2+</sup>-bound structure, the first four residues of the resulting apo structure were then extracted and protons were removed from the F1 amine and 12 and H3 backbone amides in Avogadro. A Ni<sup>2+</sup> ion was then coordinated to these nitrogens as well as the H3 sidechain  $\delta$ nitrogen. These residues were then subjected to a geometry optimization using the Universal Force Field (UFF), resulting in a square-planar geometry. Next, this structure was subjected to a second geometry optimization in Gaussian 09, [60] using the B3LYP/ 6-31+G(d) level of theory. The first three residues of this optimized structure were then re-attached to residues 4-6 of the optimized structure of apo P3 and subjected to a third geometry optimization, with residues 4-6 held fixed with the ModRedundant option. 13C and <sup>15</sup>N chemical shieldings were then calculated for each structure in Gaussian using the B3PW91/6-31 + G(d,p) level of theory and the SCRF/PCM solvent method with water as the solvent. The resultant shieldings were then related to experimental <sup>13</sup>C and <sup>15</sup>N chemical shifts by linear regression in Microsoft Excel 2016. The chemical shift differences between the metallated and unmetallated structures were calculated using a slope of -1 to relate shifts to shieldings, and compared to experimental shift differences. Unless otherwise stated, Gaussian geometry optimizations used the B3PW91/6-31+G(d) level of theory.

#### **Acknowledgements**

M.L.C. acknowledges funding from the National Science Foundation (MCB 1716608). This work was also supported by grants R35GM122501 and P41EB002031 from the National Institutes of Health and utilized the Biomedical Technology Resource Center for NMR Molecular Imaging of Proteins at the University of California, San Diego. The DFT calculations were performed in part using the College of William and Mary computing facilities,



# CHEM**PHYS**CHEM Articles

which were established through by contributions from the National Science Foundation, the Commonwealth of Virginia Equipment Trust Fund, and the Office of Naval Research.

#### Conflict of Interest

The authors declare no conflict of interest.

**Keywords:** antimicrobial peptide · magic angle spinning NMR · ATCUN motif · metallopeptide · membranes

- [1] M. Zasloff, Proc. Natl. Acad. Sci. USA 1987, 84, 5449-5453.
- [2] H. Steiner, D. Hultmark, Å. Engström, H. Bennich, H. G. Boman, *Nature* 1981, 292, 246–248.
- [3] C. D. Fjell, J. A. Hiss, R. E. W. Hancock, G. Schneider, Nat. Rev. Drug Discovery 2011, 11, 37–51.
- [4] M. Zasloff, Nature 2002, 415, 389-395.
- [5] M. Mahlapuu, J. Håkansson, L. Ringstad, C. Björn, Front. Cell. Infect. Microbiol. 2016, 6, 1–12.
- [6] R. M. Epand, H. J. Vogel, Biochim. Biophys. Acta 1999, 1462, 11-28.
- [7] E. Glukhov, M. Stark, L. L. Burrows, C. M. Deber, J. Biol. Chem. 2005, 280, 33960–33967.
- [8] W. C. Wimley, ACS Chem. Biol. 2010, 5, 905–917.
- [9] K. A. Sochacki, K. J. Barns, R. Bucki, J. C. Weisshaar, *Proc. Natl. Acad. Sci. USA* 2011, 108, E77–81.
- [10] K. A. Brogden, Nat. Rev. Microbiol. 2005, 3, 239–250.
- [11] D. Marion, M. Zasloff, A. Bax, FEBS Lett. 1988, 227, 21-26.
- [12] B. Bechinger, M. Zasloff, S. J. Opella, Protein Sci. 1993, 2, 2077–2084.
- [13] J. Gesell, M. Zasloff, S. J. Opella, J. Biomol. NMR 1997, 9, 127–135.
- [14] F. Porcelli, B. A. Buck-Koehntop, S. Thennarasu, A. Ramamoorthy, G. Veglia, *Biochemistry* 2006, 45, 5793–5799.
- [15] O. Toke, L. Cegelski, J. Schaefer, Biochim. Biophys. Acta Biomembr. 2006, 1758, 1314–1329.
- [16] E. F. Haney, H. N. Hunter, K. Matsuzaki, H. J. Vogel, Biochim. Biophys. Acta Biomembr. 2009, 1788, 1639–1655.
- [17] E. Strandberg, P. Tremouilhac, P. Wadhwani, A. S. Ulrich, Biochim. Biophys. Acta Biomembr. 2009, 1788, 1667–1679.
- [18] E. Strandberg, D. Horn, S. Reißer, J. Zerweck, P. Wadhwani, Anne S. Ulrich, *Biophys. J.* **2016**, *111*, 2149–2161.
- [19] K. Wakamatsu, A. Takeda, T. Tachi, K. Matsuzaki, Biopolymers 2002, 64, 314–327.
- [20] P. Nicolas, FEBS J. **2009**, 276, 6483–6496.
- [21] R. E. W. Hancock, H. G. Sahl, Nat. Biotechnol. 2006, 24, 1551–1557.
- [22] N. Mookherjee, R. E. W. Hancock, Cell. Mol. Life Sci. 2007, 64, 922-933.
- [23] E. F. Haney, R. E. W. Hancock, Biopolymers 2013, 6, 572–583.
- [24] S. C. Mansour, C. de la Fuente-Nunez, R. E. Hancock, J. Pept. Sci. 2015, 21, 323–329.
- [25] U. Silphaduang, E. J. Noga, Nature 2001, 414, 268-269.
- [26] M. D. J. Libardo, A. A. Bahar, B. Ma, R. Fu, L. E. McCormick, J. Zhao, S. A. McCallum, R. Nussinov, D. Ren, A. M. Angeles-Boza, M. L. Cotten, FEBS J. 2017, 284, 3662–3683.
- [27] R. M. Hayden, G. K. Goldberg, B. M. Ferguson, M. W. Schoeneck, M. D. J. Libardo, S. E. Mayeux, A. Shrestha, K. A. Bogardus, J. Hammer, S. Pryshchep, H. K. Lehman, M. L. McCormick, J. Blazyk, A. M. Angeles-Boza, R. Fu, M. L. Cotten, *J. Phys. Chem. B* 2015, 119, 15235–15246.
- [28] B. S. Perrin, Jr., Y. Tian, R. Fu, C. V. Grant, E. Y. Chekmenev, W. E. Wieczorek, A. E. Dao, R. M. Hayden, C. M. Burzynski, R. M. Venable, M. Sharma, S. J. Opella, R. W. Pastor, M. L. Cotten, J. Am. Chem. Soc. 2014, 136, 3491–3504.
- [29] C. Harford, B. Sarkar, Acc. Chem. Res. 1997, 30, 123–130.
- [30] J. C. Joyner, J. Reichfield, J. A. Cowan, J. Am. Chem. Soc. 2011, 133, 15613–15626.
- [31] G. M. Clore, Methods Enzymol. 2015, 564, 485-497.

- [32] A. Carlon, E. Ravera, W. Andralojc, G. Parigi, G. N. Murshudov, C. Luchinat, Prog. Nucl. Magn. Reson. Spectrosc. 2016, 92–93, 54–70.
- [33] C. P. Jaroniec, Solid State Nucl. Magn. Reson. 2012, 43-44, 1-13.
- [34] H. Cheng, J. L. Markley, Annu. Rev. Biophys. Biomol. Struct. 1995, 24, 209–237
- [35] J. P. Laussac, B. Sarkar, Biochemistry 1984, 23, 2832-2838.
- [36] S. Melino, M. Gallo, E. Trotta, F. Mondello, M. Paci, R. Petruzzelli, Biochemistry 2006, 45, 15373–15383.
- [37] H. Gusman, U. Lendenmann, J. Grogan, R. F. Troxler, F. G. Oppenheim, Biochim. Biophys. Acta 2001, 1545, 86–95.
- [38] S. Grzesiek, A. Bax, G. M. Clore, A. M. Gronenborn, J. S. Hu, J. Kaufman, I. Palmer, S. J. Stahl, P. T. Wingfield, Nat. Struct. Biol. 1996, 3, 340–345.
- [39] L. Cerofolini, S. Giuntini, A. Louka, E. Ravera, M. Fragai, C. Luchinat, J. Phys. Chem. B 2017, 121, 8094–8101.
- [40] M. D. J. Libardo, V. Y. Gorbatyuk, A. M. Angeles-Boza, ACS Infect. Dis. 2016, 2, 71–81.
- [41] M. D. Libardo, J. L. Cervantes, J. C. Salazar, A. M. Angeles-Boza, Chem-MedChem 2014, 9, 1892–1901
- [42] T. Miyamoto, Y. Fukino, S. Kamino, M. Ueda, S. Enomoto, *Dalton Trans.* (Cambridge, England: 2003) **2016**, 45, 9436–9445.
- [43] M. Fritz, C. M. Quinn, M. Z. Wang, G. J. Hou, X. G. Lu, L. M. I. Koharudin, T. Polenova, A. M. Gronenborn, J. Phys. Chem. B. 2017, 121, 3574–3585.
- [44] P. Vincent, S. Alina Jurca, F. Peter, New J. Chem. 2008, 32, 1189-1194.
- [45] M. R. McDonald, F. C. Fredericks, D. W. Margerum, *Inorg. Chem.* 1997, 36, 3119–3124.
- [46] R. El Meskini, V. C. Culotta, R. E. Mains, B. A. Eipper, J. Biol. Chem. 2003, 278, 12278–12284.
- [47] X. Lauth, H. Shike, J. C. Burns, M. E. Westerman, V. E. Ostland, J. M. Carlberg, J. C. Van Olst, V. Nizet, S. W. Taylor, C. Shimizu, P. Bulet, J. Biol. Chem. 2002, 277, 5030–5039.
- [48] B A Eipper, a. D A Stoffers, R. E. Mains, Annu. Rev. Neurosci. 1992, 15, 57–85.
- [49] G. Kreil, Methods Enzymol. 1984, 106, 218-223.
- [50] I. Mulero, E. J. Noga, J. Meseguer, A. Garcia-Ayala, V. Mulero, *Dev. Comp. Immunol.* 2008, 32, 1531–1538.
- [51] G. Gasmi, A. Singer, J. Forman-Kay, B. Sarkar, J. Pept. Res. 1997, 49, 500– 509.
- [52] S. Melino, C. Santone, P. Di Nardo, B. Sarkar, FEBS J. 2014, 281, 657-672.
- [53] R. S. Thakur, N. D. Kurur, P. K. Madhu, Chem. Phys. Lett. 2006, 426, 459– 463
- [54] A. Pines, M. G. Gibby, J. S. Waugh, J. Chem. Phys. 1972, 56, 1776–1777.
- [55] N. Bloembergen, Physica 1949, 15, 386-426.
- [56] M. H. Frey, S. J. Opella, J. Am. Chem. Soc. **1984**, 106, 4942–4945.
- [57] N. M. Szeverenyi, M. J. Sullivan, G. E. Maciel, J. Magn. Reson. 1982, 47, 462–475.
- [58] M. Baldus, A. T. Petkova, J. Herzfeld, R. G. Griffin, Mol. Phys. 1998, 95, 1197–1207.
- [59] M. D. Hanwell, D. E. Curtis, D. C. Lonie, T. Vandermeersch, E. Zurek, G. R. Hutchison, J. Cheminf. 2012, 4.
- [60] M. J. Frisch, G. W. Trucks, H. B. Schlegel, G. E. Scuseria, M. A. Robb, J. R. Cheeseman, G. Scalmani, V. Barone, B. Mennucci, G. A. Petersson, H. Nakatsuji, M. Caricato, X. Li, H. P. Hratchian, A. F. Izmaylov, J. Bloino, G. Zheng, J. L. Sonnenberg, M. Hada, M. Ehara, K. Toyota, R. Fukuda, J. Hasegawa, M. Ishida, T. Nakajima, Y. Honda, O. Kitao, H. Nakai, T. Vreven, J. J. A. Montgomery, J. E. Peralta, F. Ogliaro, M. Bearpark, J. J. Heyd, E. Brothers, K. N. Kudin, V. N. Staroverov, T. Keith, R. Kobayashi, J. Normand, K. Raghavachari, A. Rendell, J. C. Burant, S. S. Iyengar, J. Tomasi, M. Cossi, N. Rega, J. M. Millam, M. Klene, J. E. Knox, J. B. Cross, V. Bakken, C. Adamo, J. Jaramillo, R. Gomperts, R. E. Stratmann, O. Yazyev, A. J. Austin, R. Cammi, C. Pomelli, J. W. Ochterski, R. L. Martin, K. Morokuma, V. G. Zakrzewski, G. A. Voth, P. Salvador, J. J. Dannenberg, S. Dapprich, A. D. Daniels, O. Farkas, J. B. Foresman, J. V. Ortiz, J. Cioslowski, D. J. Fox in Gaussian 09 Rev. E.01, Vol. (Ed. Eds.: Editor), City, 2009

Manuscript received: September 8, 2018 Revised manuscript received: November 21, 2018 Version of record online: December 19, 2018